applied sciences

MDPI

Article

Surface Charge and Phosphorus Retention in Metal-Activated Biochars from Different Pyrolysis Temperatures

Sofia Maria Muscarella [1], Luigi Badalucco [1], Vito Armando Laudicina [1,2,*] and Pellegrino Conte [1,3]

[1] Department of Agricultural, Food and Forest Sciences, University of Palermo, Viale delle Scienze, Building 4, 90128 Palermo, Italy; sofiamaria.muscarella@unipa.it (S.M.M.); luigi.badalucco@unipa.it (L.B.); pellegrino.conte@unipa.it (P.C.)
[2] National Biodiversity Future Center (NBFC), Piazza Marina, 61, 90133 Palermo, Italy
[3] Consorzio Interuniversitario Nazionale per la Scienza e Tecnologia dei Materiali (INSTM), Via G. Giusti, 9, 50121 Firenze, Italy
* Correspondence: vitoarmando.laudicina@unipa.it

Abstract

Biochar is a promising material for phosphorus (P) removal from water, but its surface chemistry can limit adsorption efficiency. In this study, biochars produced at 440 °C and 880 °C from the same feedstock were functionalized post-pyrolysis using aqueous solutions of $AlCl_3$, $CaCl_2$, and $FeCl_3$ at two concentrations (0.5 M and 2.0 M). The aim of this work was to assess how both pyrolysis temperature and post-pyrolysis activation with different metals affect the surface charge of biochar and its capacity to retain P from aqueous solution. The treated materials were characterized for pH, point of zero charge (pH_{pzc}), and phosphorus retention from solution. Results showed that Al- and Fe-activation significantly reduced the biochar pH and shifted the pH_{pzc} to more acidic values, enhancing electrostatic attraction toward phosphate species. Phosphorus adsorption was most effective for biochar obtained at 440 °C and treated with $AlCl_3$ and $FeCl_3$, achieving up to 10.2 mg P g^{-1}. These findings highlight the importance of surface charge modulation in tuning biochar performance for phosphate removal from aqueous solution. Based on the obtained results, electrostatic attraction was the main mechanism by which activated biochar adsorbed P from aqueous solution.

Keywords: biochar; post-pyrolysis activation; phosphorus adsorption; $AlCl_3$; $FeCl_3$; pH_{pzc}; electrostatic interactions

Academic Editor: Juan García Rodríguez

Received: 20 June 2025
Revised: 1 August 2025
Accepted: 9 August 2025
Published: 11 August 2025

Citation: Muscarella, S.M.; Badalucco, L.; Laudicina, V.A.; Conte, P. Surface Charge and Phosphorus Retention in Metal-Activated Biochars from Different Pyrolysis Temperatures. *Appl. Sci.* **2025**, *15*, 8855. https://doi.org/10.3390/app15168855

Copyright: © 2025 by the author. Licensee MDPI, Basel, Switzerland. This article is an open access article distributed under the terms and conditions of the Creative Commons Attribution (CC BY) license (https://creativecommons.org/licenses/by/4.0/).

1. Introduction

Phosphorus (P) is a fundamental nutrient for plant growth and a critical element for all life [1]. Due to its essential role in agriculture, global demand for phosphate-based fertilizers continues to increase [2]. However, phosphorus is a finite resource, and current consumption trends suggest that known reserves could be depleted within the next 400 years [3]. Europe faces vulnerability, as it depends entirely on imported phosphorus, a situation exacerbated by geopolitical instability and global conflicts [4]. As a result, identifying sustainable and locally available phosphorus sources has become an urgent priority.

Treated wastewater (TWW) represents a viable and underutilized source of recoverable phosphate [5]. Modern wastewater treatment involves multiple stages, including primary and secondary treatment to remove solids and organic matter, with advanced facilities also implementing tertiary processes to eliminate nutrients and heavy

metals [6]. Despite these treatments, TWW can still contain phosphate concentrations as high as 10 mg L^{-1} [7,8]. Various methods have been explored for phosphate recovery, including biological uptake, chemical precipitation, and adsorption-based techniques [9,10]. Among these, adsorption has gained significant attention due to its cost-effectiveness, operational simplicity, and high efficiency, particularly at low phosphate concentrations [11]. Column studies with real ultrafiltered wastewater have already demonstrated the feasibility of phosphate removal using biochar [12,13]. An additional advantage is that spent adsorbents enriched with phosphorus can be repurposed as slow-release fertilizers, supporting circular economy principles [14–16].

Biochar has emerged as a promising adsorbent for phosphate recovery. Produced through the thermal decomposition of biomass under oxygen-starved conditions, typically at temperatures between 300 and 800 °C [17,18], biochar possesses a highly porous structure, substantial surface area (up to 1000 m^2 g^{-1}), and low density [19,20]. Studies have demonstrated that biochars derived from various feedstocks, such as wood, rice husk, and sewage sludge, can achieve phosphate adsorption capacities ranging from 15 to 117 mg PO_4^{3-} g^{-1} [21–24]. Nevertheless, untreated biochar often exhibits limited adsorption performance because its negatively charged surface repels anionic phosphate species [23].

To enhance adsorption, recent studies have further explored P recovery using biochar subjected to chemical activation. This process is generally more effective than physical or biological treatments [25] and can involve acid or alkaline modification [24,26,27], carboxylation, or impregnation with metal oxides [16,18,28–30]. Of these methods, loading biochar with polyvalent metals, either before or after pyrolysis, has proven particularly effective, as it introduces cationic sites that strongly bind phosphate [31–34]. While pre-pyrolysis metal impregnation is common, it requires specialized equipment and can be costly. In contrast, post-pyrolysis activation offers a more flexible and scalable alternative. For instance, Choi et al. [31] demonstrated that coating dairy manure-derived biochar with calcium hydroxide after pyrolysis increased phosphate removal from 23% to 89%. Similarly, Zheng et al. [35] and Zhong et al. [36] reported significant improvements in phosphate uptake using aluminum- and iron-modified biochars, with the latter achieving adsorption capacities up to 36 mg P g^{-1}.

Despite these advances, key knowledge gaps remain. Few studies have systematically examined how post-pyrolysis metal activation influences biochar surface charge and phosphate adsorption mechanisms, although some recent works have begun to address this gap [21,35–37]. Additionally, conventional batch experiments often estimate phosphate removal based solely on solution depletion, neglecting potential precipitation with leached metal ions. This oversight may lead to an overestimation of true adsorption capacity. To our best knowledge, this is the first study to systematically compare the combined effects of pyrolysis temperature and post-pyrolysis metal activation on biochar surface charge and phosphate adsorption, providing novel insights into phosphate removal mechanisms. Here, activation refers to the post-pyrolysis impregnation of the biochar surface with metals supplied by various saline solutions, thereby creating adsorption sites for phosphate. This study evaluates the phosphate adsorption performance of biochar activated post-pyrolysis with three metal chlorides ($AlCl_3$, $CaCl_2$, $FeCl_3$) at two concentrations (0.5 and 2.0 M). We also investigated the effect of pyrolysis temperature (440 °C and 880 °C) on adsorption efficiency. Our hypotheses are: (i) metal-activated biochars adsorb more phosphorus than non-activated biochars, and (ii) adsorption capacity increases with the valence of the loaded metal cation. By directly quantifying phosphorus retained on the biochar surface, rather than relying solely on solution measurements, we aim to provide a more accurate assessment of adsorption performance.

2. Materials and Methods

2.1. Biomass Pyrolysis for Biochar Production

Woody biomass from the pruning residues of the green areas of the Palermo University Campus (38°06′25.8″ N 13°21′07.7″ E) was used as a raw material to produce biochar. Before pyrolysis, the woody biomass was cut into pieces of <5 cm and washed sequentially with deionized water to minimize dust, followed by overnight drying in an air oven at 60 °C. The residual dry biomass was ground to <5 mm and used to prepare biochar. The ground material was placed into a sealed porcelain container and burnt in a muffle furnace for 3 h at 440 °C or 880 °C under a 5 mL min^{-1} N_2 flow to reduce oxygen concentration. The biochars produced were collected and named B440 and B880, respectively. The main characteristics of the two biochars are reported in Table 1.

Table 1. Physical and chemical properties of the two tested biochars (B440 and B880). Reported values are mean ± standard deviations of three replicates.

Parameters	B440	B880
Bulk density (g L^{-1})	180 ± 14	126 ± 11
Surface area (m^2 g^{-1})	194 ± 12	247 ± 15
Cation exchange capacity (×10^{-2} mol kg^{-1})	14 ± 1	12 ± 1
Total pore volume (cm^3 g^{-1})	38 ± 4	51 ± 3
Maximum water retention (%)	62 ± 11	400 ± 32
Reaction (pH)	9 ± 1	10 ± 1
Electrical conductivity (dS m^{-1})	1.3 ± 0.2	2.1 ± 0.3
Moisture (%)	3.1 ± 0.3	7 ± 1
Total limestone (%)	5.0 ± 0.8	2.7 ± 0.3
Total carbon (%)	65 ± 4	72 ± 5
Ashes to 550 °C (%)	3.4 ± 0.3	6.4 ± 0.6
Molar ratio H:C	0.7 ± 0.2	0.2 ± 0.1

2.2. Preparation of Activated Biochar

Before use, all the biochars were sieved at ø 2–5 mm, washed trice with distilled water (200 g of each biochar with 1.5 L) to remove particulate impurities, and dried at 60 °C for 72 h. Then, biochar was pre-treated with hydrochloric acid (HCl). Thus, 150 g of each dried biochar was shaken on a horizontal shaker for 12 h at 60 rpm with 1 M HCl solution (1:5 ratio, *w* v^{-1}).

Finally, biochars were washed once with distilled water (1:2.5 ratio, *w* v^{-1}) and dried at 60 °C for 72 h. Following such pre-treatments, aliquots (15 g) of each biochar were activated by soaking it with different salt solutions at a biochar: solution ratio of 1:20 (*w* v^{-1}) [33]. The salts used to prepare 0.5 and 2.0 M solutions were calcium chloride ($CaCl_2$), aluminum chloride ($AlCl_3$), and iron chloride ($FeCl_3$) [35,36]. The salts were analytical grade, all purchased from Sigma Aldrich (Milan, Italy). The treatments of the biochars with 0.5 and 2.0 M $FeCl_3$ solutions at 80 °C for 6 h [36]. All the biochar was shaken with a salt solution for 48 h at 60 rpm. Afterwards, activated biochars were washed three times with 50 mL of distilled water (1:2.5 ratio, *w* v^{-1}) by hand shaking for 3 min; the water was discharged and, finally, dried at 60 °C for 72 h to remove residual moisture and promote partial conversion of metal salts to metal oxides [38]. Notably, $FeCl_3$ and $AlCl_3$ solutions are acidic (pH ≈ 1–2 at 2.0 M), which helps neutralize the alkalinity of biochar and dissolve carbonates, thereby facilitating metal ion uptake onto the biochar. In contrast, $CaCl_2$ solutions are neutral, so Ca^{2+} impregnation occurs without significant changes in the pH of the biochar surface.

2.3. Characterisation of Biochar by ATR-FTIR

A Perkin-Elmer Spectrum Two FTIR spectrometer equipped with an attenuated total reflectance device was used for acquiring the Fourier Transform Infrared-Attenuated Total Reflectance (ATR-FTIR) spectra of all biochar samples. Such spectra were acquired to assess the main functional groups of the tested biochar. Approximately 1 mg of pulverized biochar was used to obtain the spectra in the wavenumber range 3600–600 cm^{-1}, with a resolution of 4 cm^{-1} and 32 scans, according to Sharma et al. [39]. Furthermore, the presence of P as a result of absorption on biochar was assessed by observing changes in the band between 1190 and 600 cm^{-1} as suggested by Zhou et al. [40]. The spectra have been elaborated by using the PerkinElmer Spectrum (Version 10.5.1) software program.

2.4. Determination of Cation Exchange Capacity (CEC) and Metals Absorbed by Biochar

Biochar CEC was measured according to Munera-Echeverri et al. [41]. Briefly, 1 g of biochar was shaken with 20 mL 1 M NH_4OAc (Ammonium acetate, analytical grade) buffered at pH 7. After 24 h, the suspension was filtered through Whatman paper 42 filters, and CEC was calculated as the sum of exchangeable base cations (Ca^{2+}, Mg^{2+}, K^+, Na^+) determined by microwave plasma atomic emission spectroscopy (MP-AES 4210, Milan, Italy).

Metals (i.e., Al, Ca, Fe) absorbed by biochar were determined by elemental analyses after acid digestion of the biochar [42]. Briefly, 250 mg of each biochar was pulverized and digested using 3 mL of HNO_3 and 5 mL of H_2O_2. The excess of HNO_3 and H_2O_2 were evaporated by hot plate at 125 °C and then, samples were placed in muffle at 500 °C for 8 h. Analytical grade concentrated nitric acid (HNO_3, 67–69% *v* v^{-1}) and hydrogen peroxide (H_2O_2, 30% *v* v^{-1}) purchased from Sigma-Aldrich (Milan, Italy) were used for sample digestion [36]. Digested samples were recovered with a 2% nitric acid solution and analysed by MP-AES to determine the amount of Ca, Fe, and Al.

2.5. Determination of pH and pH Value at Zero-Point Charge of Biochars

After 24 h of contact, the reaction of the P-solution (1000 mg P L^{-1} from K_2HPO_4) in contact with biochars (B440 and B880, respectively) was determined by a pH-meter (FiveEasy, Mettler Toledo Spa, Milan, Italy) equipped with a glass electrode. The point of zero charge (pH_{pzc}) of biochars (B440 and B880, respectively) was evaluated using the pH drift method according to Nasiruddin et al. [43] as described in Vaičiukyniene et al. [44]. Sodium chloride (0.01 M) was used as a background electrolyte. Eight solutions with pH values ranging from 2 to 9 were prepared by adjusting the pH by adding small amounts of 0.5 M HCl or 0.5 M NaOH solutions. Then, 0.1 g of each biochar was soaked with 40 mL of each solution and left to settle for 24 h at room temperature. The final pH of each solution was measured. The pH_{pzc} of biochar was evaluated as follows: if the initial pH of the solution was equal to the final pH of the solution, then that was considered the pH_{pzc}, and the charge on the biochar surface was supposed to be zero [44].

2.6. Phosphate Absorption by Biochar

Two grams of not-treated, HCl pre-treated, and metal-activated biochar were immersed in 100 mL of a 1000 mg P L^{-1} solution prepared using dipotassium monohydrogen phosphate (K_2HPO_4). Biochars were shaken on a horizontal shaker for 24 h at 80 rpm. Then, they were separated from the solution by filtration using 42 Whatman paper filters, washed trice with distilled water (1:2.5 ratio, *w*:*v*), and dried at 60 °C for 72 h. Samples of the solutions were employed to measure the pH of the P solution after contact with the biochar samples using a pH meter (FiveEasy, Mettler Toledo Spa, Milan, Italy). Biochar samples were used for FTIR analysis to quantify the amount of absorbed P.

2.7. Phosphate Determination

The amount of P absorbed by biochars was determined as follows: biochar samples were pulverized in a porcelain mortar, and the resulting ground materials (0.25 g) underwent mineralization in porcelain crucibles within a muffle furnace at 550 °C for 8 h.

The resulting ashes were suspended by using 1 M HCl on a hotplate at 100 °C for 10 min. The digested samples were recovered in 15 mL tubes and adjusted to 10 mL of volume with MilliQ grade water. P concentration was then determined using the colorimetric method [45] by a spectrophotometer (UVmini-1240, Shimadzu Italia srl, Milan, Italy) at 882 nm.

2.8. Phosphate Adsorption Isotherms and Model Fitting

Phosphorus (P) adsorption performance of the most efficient biochars was evaluated through isotherm modeling, with the aim of characterizing the interaction between phosphate ions and the porous surface of activated materials. Adsorption isotherms provide valuable information on surface properties such as the affinity of the adsorbent, energetic heterogeneity, and the distribution of adsorption sites. Furthermore, they allow the comparison and classification of biochars based on differences in surface chemistry, mineral composition, and activation treatments. In this study, three isotherm models were applied: the Freundlich, Langmuir, and Langmuir–Sips [46–49].

The Freundlich model is empirical and assumes adsorption on a heterogeneous surface with non-uniform energies and multilayer formation. Its equation is:

$$q_e = K_F C^{1/n} \quad (1)$$

where q_e is the amount of P adsorbed per unit mass of biochar (mg g^{-1}), C is the equilibrium concentration of phosphate in solution (mg L^{-1}), on, K_F is the Freundlich constant related to adsorption capacity, and n is an empirical factor linked to surface heterogeneity [50].

The Langmuir model describes monolayer adsorption on a surface with a finite number of identical and energetically equivalent binding sites, according to:

$$q_e \propto \frac{K_L C}{K_L C + 1} \quad (2)$$

Here, q_e and C have the same meaning as in Equation (1), while K_L is the Langmuir equilibrium constant. To account for deviations from ideal conditions and better represent surface heterogeneity, the Langmuir Equation (2) can be modified as in Equation (3):

$$q_e \propto \frac{K_L C^n}{K_L C^n + 1} \quad (3)$$

where the exponent n reflects the influence of adsorbate concentration on site occupancy and energetic distribution.

Equation (1) assumes a heterogeneous surface with a non-uniform distribution of heat of adsorption over the surface and binding sites are not equivalent and/or independent [49]. Equation (2) is valid for monolayer adsorptions on a surface with a finite number of identical sites. However, Equation (3) can be further generalized into the Langmuir–Sips model, which incorporates both the Freundlich and Langmuir behaviors and is written as:

$$q_e = \frac{q_{max} K_S C^n}{K_S + 1} \quad (4)$$

In this expression, q_{max} is the maximum adsorption capacity, K_S is the Sips constant (analogous to K_L), and n is the heterogeneity exponent (18,51). When n =1, Equation (4) reduces to the Langmuir isotherm (Equation (2)); when $K_S \rightarrow 0$, it approaches the Freundlich form (Equation (1)). This flexibility makes the Langmuir–Sips model particularly suitable for materials with complex surface characteristics.

Data for P adsorption isotherms were conducted by shaking 1 g of biochar in 100 mL of phosphate solution (KH_2PO_4) at initial concentrations of 10, 25, 50, 100, 250, 500, 750, and 1000 mg P L^{-1}. The suspensions were sealed in polyethylene tubes and agitated on a horizontal shaker at 80 rpm at room temperature (22 ± 1 °C) for 24 h, a contact time previously established to ensure adsorption equilibrium. After equilibration, the suspensions were filtered through Whatman Grade 42 ashless filter paper, and the residual phosphate concentration in solution was determined using the molybdenum blue colorimetric method [45]. Absorbance readings were performed at 882 nm with a Shimadzu UVmini-1240 spectrophotometer. All measurements were conducted in triplicate. The P adsorbed on biochar, determined by Berthelot colorimetric method, was fitted to the Freundlich (Equation (1)), Langmuir, and Langmuir-Sips equations. All the isotherms were calculated by using non-linear regression with the Origin (Version 7.5) software program. The quality of the fits was evaluated using the R^2 and the chi-square statistic (χ^2).

3. Results

3.1. ATR-FTIR Spectra of B440 and B880 Biochars

The FTIR spectra of both untreated and activated B440 and B880 biochars, shown in Figure 1, displayed similar patterns, with absorption bands typically found in biochars derived from lignocellulosic biomass [51].

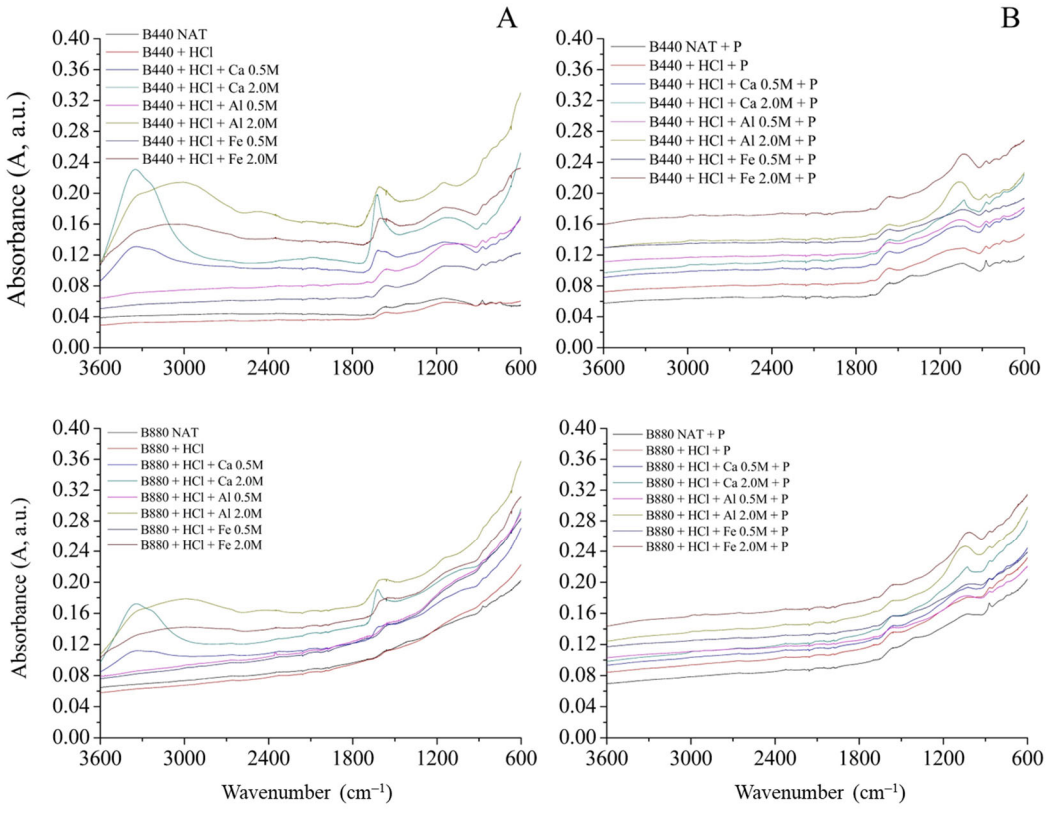

Figure 1. ATR-FTIR spectra of biochars (B440 and B880) in the range 3600–600 cm^{-1} wavenumber: (**A**) Not P-enriched; (**B**) P-enriched.

The broad band observed around 3400 cm^{-1} is generally associated with O–H stretching. In this case, it is likely due to adsorbed water rather than phenolic groups, since such functionalities tend to decrease at higher pyrolysis temperatures due to graphitization processes [52].

In the region between 1700 and 1300 cm^{-1}, the spectra show bands related to C=O stretching in carboxylic and carbonyl groups. Normally, when biochar interacts with metal ions, one would expect these peaks to decrease in intensity or shift due to coordination with COOH groups [53]. However, in this study, an increase in peak intensity after chloride salt treatments was observed. This could suggest some surface chemistry changes or even the presence of residual ions not fully removed during washing. A similar effect has been described by Guo et al. [54], where HCl treatment led to the removal of carbonates and improved sorption properties of biochar. In general, acid treatment can modify the surface area, introduce new functional groups, and enhance selectivity for certain adsorbates [55,56].

That said, the results observed here are a bit counterintuitive when considering the pyrolysis temperature. As pyrolysis temperature increases, the carbon structure becomes more aromatic and graphitic, and oxygen-containing groups such as hydroxyls and carboxyls tend to disappear; these are usually key sites for metal ion binding [52]. Therefore, we would expect less interaction with metal salts in high-temperature biochars. The increase in the 1700–1300 cm^{-1} band intensity after treatment might then be due more to loosely bound ions or side reactions on the surface, rather than strong coordination with functional groups [53].

After phosphate adsorption, a slight decrease in peak intensity was noted near 1700 and 1300 cm^{-1}. This could point to some competition between phosphate species and the previously introduced metal-functional group complexes [35,57]. A band around 1100 cm^{-1} was also observed, which is often associated with P=O stretching or O–C vibrations in P–O–C linkages [58]. However, under the experimental conditions used here, the formation of covalent P–C bonds is unlikely. It is more plausible that this signal reflects the presence of adsorbed phosphate species (like $H_2PO_4^-$ or HPO_4^{2-}) rather than any newly formed organophosphorus structures, which would require much more energy to generate.

3.2. Metal Absorption by Biochars

After HCl treatment, both biochars showed a noticeable decrease in metal content compared to the untreated samples. This reduction has already been reported in previous studies [41,54], and it is generally attributed to the loss of surface-bound salts and the dissolution of residual carbonates. When the biochars were subsequently soaked in chloride salt solutions, they reabsorbed metals, sometimes in quantities even higher than those originally measured in the untreated biochars (Table 2). Interestingly, the two biochars responded differently to the salt treatments. After exposure to 0.5 M chloride solutions, B440 did not show a meaningful increase in metal content compared to its untreated counterpart. Conversely, B880 absorbed significantly more metal: aluminum and iron contents were approximately 33% and 44% higher, respectively, than in the untreated sample.

When the chloride concentration was increased to 2.0 M, both biochars absorbed metal in much larger amounts: at least an order of magnitude more than the untreated controls. This suggests a clear trend, that is, higher salt concentrations lead to more effective metal uptake (Table 2).

The difference in metal absorption between B440 and B880 could be related to their electrostatic properties. After HCl treatment, B880 exhibited a slightly higher cation exchange capacity ($12.1 \pm 0.6 \times 10^{-2}$ mol^+ kg^{-1}) than B440 ($10.1 \pm 0.6 \times 10^{-2}$ mol^+ kg^{-1}), which may enhance its ability to retain positively charged metal ions. Still, other mechanisms such as complexation, precipitation, or even physical entrapment of metal salts cannot be ruled out [19].

Table 2. Concentration of calcium (Ca), aluminum (Al), and iron (Fe) in biochars (B440 and B880) activated with 0.5 M or 2.0 M $CaCl_2$, $AlCl_3$, and $FeCl_3$ salt solutions. The reported results are mean ± standard deviations of three replicates. n.d., not determined.

Treatment	Al	Ca	Fe
	mg g^{-1}	mg g^{-1}	mg g^{-1}
B440 NAT	0.6 ± 0.2	8 ± 1	5 ± 1
B440 + HCl	0.3 ± 0.2	4 ± 1	1.5 ± 0.1
B440 + HCl + Al 0.5 M	0.8 ± 0.2	n.d.	n.d.
B440 + HCl + Ca 0.5 M	n.d.	6 ± 1	n.d.
B440 + HCl + Fe 0.5 M	n.d.	n.d.	1.2 ± 0.2
B440 + HCl + Al 2.0 M	8 ± 1	n.d.	n.d.
B440 + HCl + Ca 2.0 M	n.d.	28 ± 3	n.d.
B440 + HCl + Fe 2.0 M	n.d.	n.d.	13 ± 1
B880 NAT	0.3 ± 0.1	6 ± 1	2.7 ± 0.5
B880 + HCl	0.2 ± 0.1	2.2 ± 0.4	1.2 ± 0.3
B880 + HCl + Al 0.5 M	1.3 ± 0.4	n.d.	n.d.
B880 + HCl + Ca 0.5 M	n.d.	8 ± 1	n.d.
B880 + HCl + Fe 0.5 M	n.d.	n.d.	3.9 ± 0.4
B880 + HCl + Al 2.0 M	14 ± 2	n.d.	n.d.
B880 + HCl + Ca 2.0 M	n.d.	29 ± 3	n.d.
B880 + HCl + Fe 2.0 M	n.d.	n.d.	17 ± 2

3.3. Effect of HCl and Metal Salt Treatments on Phosphorus Adsorption

Phosphate adsorption by biochar is influenced by several factors [24]. After HCl treatment, B440 showed about 25% less phosphorus compared to the untreated sample. This drop may be due to the rinsing away of surface particles or the removal of carbonated species, which could otherwise trap or interact with phosphate ions. Interestingly, when this HCl-treated biochar was placed back into phosphate solution, it ended up absorbing 40% more P than it had originally retained, thereby suggesting that the acid treatment improved its capacity for phosphate uptake. That said, the overall adsorption was still relatively low compared to values reported in similar studies. For instance, Li et al. [55] found that biochar treated with 6 mol L^{-1} HCl showed a 6% increase in P uptake over untreated biochar.

When comparing activated biochars to the HCl-only control, the improvement in phosphate adsorption was much more pronounced. After treatment with 0.5 M $CaCl_2$, $AlCl_3$, or $FeCl_3$, B440 absorbed 165%, 368%, and 456% more P, respectively. B880 performed even better, with P uptake increases of 524%, 414%, and 551%, respectively, compared to the control. Moreover, increasing the chloride salt concentration to 2.0 M further boosted the amount of P adsorbed: B440 gained 42%, 49%, and 79%, while B880 showed increases of 1%, 122%, and 76%, relative to their corresponding 0.5 M treatments. In absolute terms, the amount of P retained ranged from 2% to 20% of the initial phosphorus present in the solution (Figure 2).

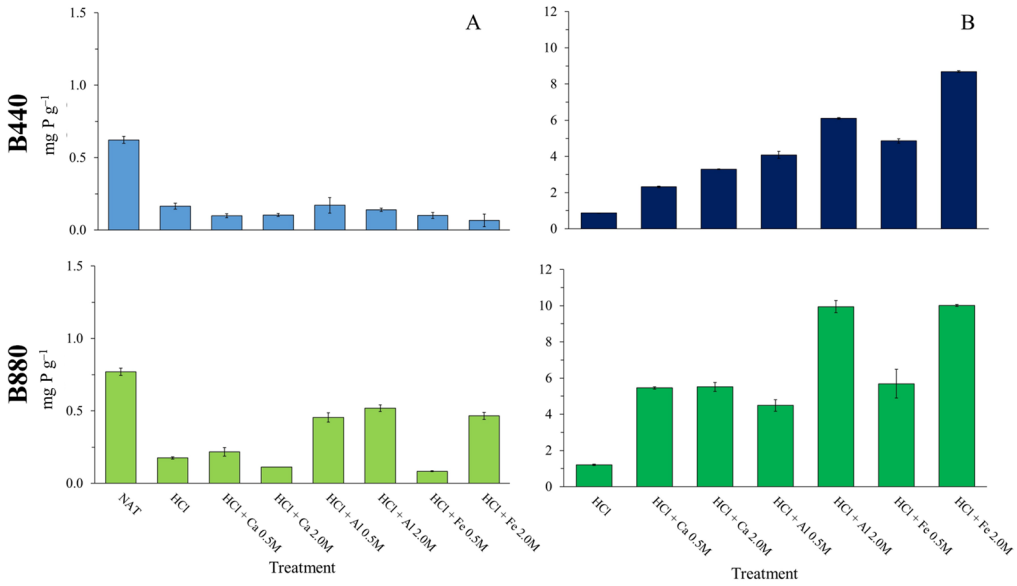

Figure 2. Amount of P in activated and not activated biochars (B440 and B880) before (**A**) and after (**B**) their contact for 24 h with a mono-component solution (1000 mg P L^{-1} of K_2HPO_4). Note different y-axis scales.

These values are clearly lower than those found in other works, where P adsorption on biochar ranged from 82 to 111 mg g^{-1} [17,24,59,60]. This could be due to the experimental method used here, which is closer to that applied in studies on phosphate retention by other solid substrates [24,61–63]. In this study, biochar was washed with water after exposure to phosphate solution, which may have removed loosely bound or surface-precipitated P. This step, while possibly causing some losses, is actually more reliable than simply measuring P removal from solution, an approach that does not account for labile forms or precipitation occurring in the test flask. In this light, the stronger P adsorption seen with increasing salt concentrations may be attributed to the higher metal content on the biochar surface (Table 2), which also influences the pH of the solution in contact with the material.

3.4. Influence of Solution pH and Surface Charge on P Adsorption

The pH of the solution in contact with activated biochars turned out to be a key factor in determining how much phosphorus was actually adsorbed. This is because pH affects not only the speciation of phosphate in solution, but also the surface properties of the adsorbent, especially surface charge and the behavior of functional groups [64]. After 24 h of contact, the pH values of the solutions had shifted, as shown in Table 3.

For B440, the amount of P retained ranged from 0.9 to 8.7 mg g^{-1}, corresponding to a solution pH of 7.1 and 1.4, respectively. B880 showed similar behavior, with values from 1.2 to 10.0 mg g^{-1} at pH 7.8 and 1.2, respectively. As reported in Figure 3, this resulted in a clear negative correlation between solution pH and the amount of phosphate adsorbed: the lower the pH, the greater the adsorption. It is important to note that phosphate speciation is pH-dependent: in strongly acidic conditions (pH < 2) the dominant form is H_3PO_4, at mildly acidic to neutral pH (≈2–7) $H_2PO_4^-$ prevails; at neutral to moderately basic pH (≈7–12) the primary species is HPO_4^{2-}; and under highly basic conditions (pH > 12) PO_4^{3-} becomes dominant. In our experiments, the solution pH after biochar contact ranged from 1.4 to 7.1 (Table 3), suggesting that the phosphate was present mostly as $H_2PO_4^-$ (with some HPO_4^{2-} at the higher pH end).

Table 3. pH value of the P-solution after 24 h contact with biochars (B440 and B880). Values are mean ± standard deviations of three replicates.

Sample	pH
B440 NAT	9.1 ± 0.1
B440 + HCl	7.1 ± 0.1
B440 + HCl + Ca 0.5 M	6.1 ± 0.3
B440 + HCl + Ca 2.0 M	4.9 ± 0.2
B440 + HCl + Al 0.5 M	4.9 ± 0.3
B440 + HCl + Al 2.0 M	2.4 ± 0.1
B440 + HCl + Fe 0.5 M	5.1 ± 0.4
B440 + HCl + Fe 2.0 M	1.4 ± 0.1
B880 NAT	10.1 ± 0.2
B880 + HCl	7.8 ± 0.1
B880 + HCl + Ca 0.5 M	6.5 ± 0.2
B880 + HCl + Ca 2.0 M	5.2 ± 0.1
B880 + HCl + Al 0.5 M	7.1 ± 0.3
B880 + HCl + Al 2.0 M	2.7 ± 0.2
B880 + HCl + Fe 0.5 M	5.6 ± 0.1
B880 + HCl+ Fe 2.0 M	1.2 ± 0.4

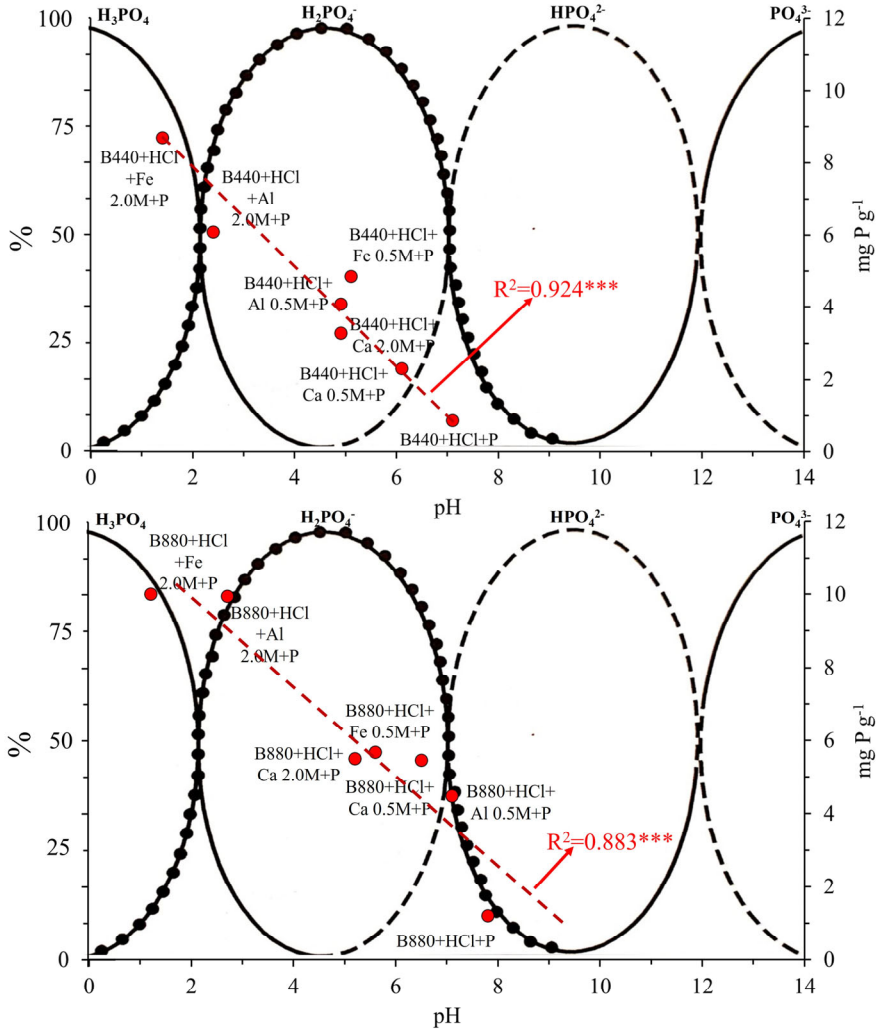

Figure 3. The relationship between the amount of P absorbed by biochars (B440 and B880) and the pH of the aqueous solution overlaps with the diagram of P species in relation to the pH of the aqueous solution. Asterisks indicate significance levels: $p < 0.001$ (***). This trend is consistent with

previous studies [55,63]. When the solution pH is low, surface functional groups, especially carboxyl and hydroxyl groups, tend to be protonated. Also, the metals present on the surface, like Ca, Al, or Fe, can form positively charged species such as $CaOH^+$, $Al(OH)_2^+$, or $Fe(OH)_2^+$. These positively charged sites are able to attract anionic phosphate species like HPO_4^{2-} and $H_2PO_4^-$ via electrostatic interactions. As the pH increases, these groups deprotonate, and the surface becomes more negatively charged. This leads to repulsive interactions between the phosphate anions and the negatively charged surface, which limits adsorption [65,66].

To better understand this behavior, the point of zero charge (pH_{pzc}) was measured for all biochars. This parameter is essential to anticipate whether a biochar surface will attract or repel phosphate under certain pH conditions. When the solution pH is lower than the pH_{pzc}, the biochar surface is positively charged, favoring phosphate retention through electrostatic attraction. When the pH is higher, the surface becomes negatively charged, and repulsion dominates.

In this study, B440 had a pH_{pzc} between 5.5 and 7, while biochar treated with 2.0 M $FeCl_3$ revealed a much lower value: below 2 (Figure 4). B880 showed a slightly higher pH_{pzc} overall, ranging from 6.2 to 7.3 for the Ca-treated samples, and from 3.5 down to less than 2 for Al- and Fe-treated biochars.

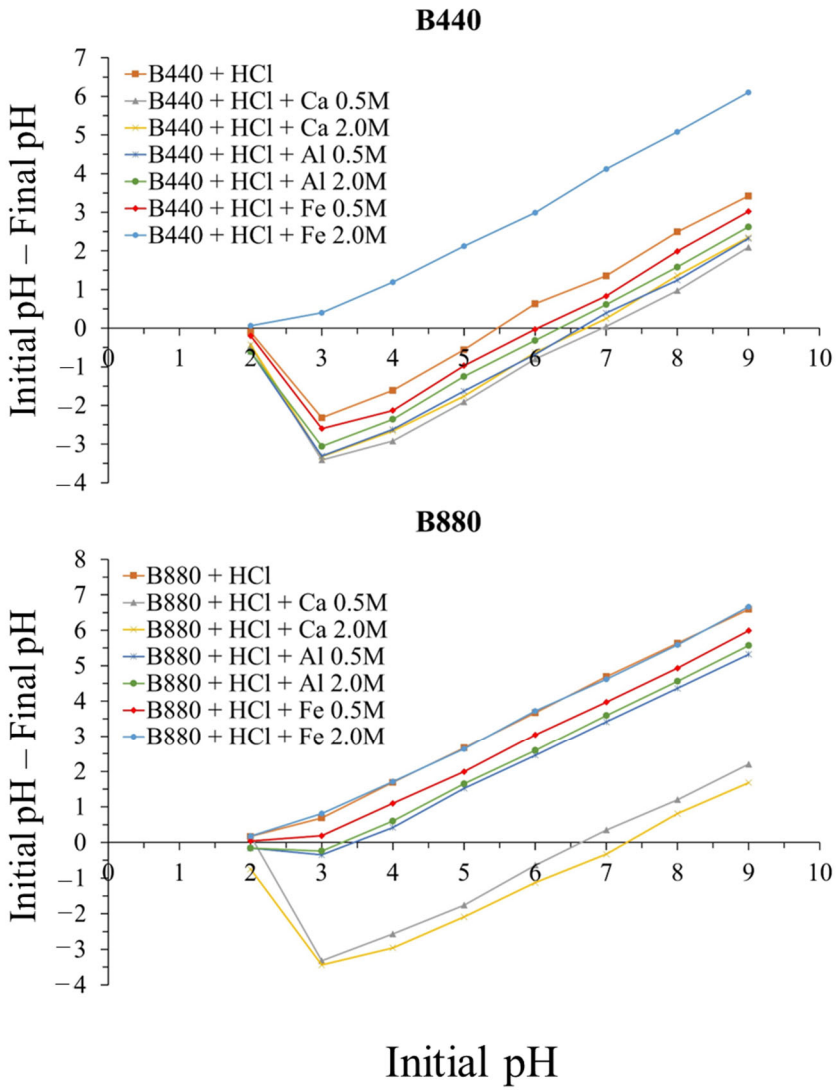

Figure 4. Point of zero charge (pH_{pzc}) of biochars B440 and B880 after activation with different salt treatments.

This pattern helps explain why biochars treated with HCl had the lowest phosphate adsorption: their pH_{pzc} values were below 5.5, and the solution pH was always higher than 7.1 (Table 3). On the other hand, the highest adsorption was recorded for the two biochars treated with 2.0 M $FeCl_3$, which had a very low pH_{pzc} (<2) and were in contact with solutions with pH below 1.4. This behavior can be attributed to electrostatic interactions between the negatively charged phosphate species and positively charged surface sites formed by metal hydroxides. These observations align with Eduah et al. [27], who reported maximum phosphate uptake for Fe-activated biochars at around pH 3. At higher pH values, phosphate removal dropped, likely due to increased OH^- competition and a negatively charged surface. A similar effect was observed by Yang et al. [67].

3.5. Mechanistic Interpretation Based on FTIR Evidence

Based on all these findings, it seems that the main mechanism responsible for phosphorus retention in activated biochars is electrostatic attraction between negatively charged phosphate species and the cation-enriched surface of the biochar. This hypothesis is also supported by the ATR-FTIR spectra.

In particular, the broad peak around 3400 cm^{-1}, typically associated with phenol -OH groups, disappeared after exposure to phosphate solution, which suggests that these groups may have played a role in the adsorption process. At the same time, a stronger peak appeared near 1100 cm^{-1}, which is consistent with the presence of phosphate species retained on the surface [58].

Moreover, the bands between 1700 and 1300 cm^{-1}, which are usually attributed to carboxylic functional groups, showed a decrease in intensity after phosphate adsorption. This is in line with the mechanism proposed by Eduah et al. [27], who suggested that protonated phenol and carboxylic groups can act as adsorption sites for anionic phosphate species through electrostatic interactions.

Even when the same chloride salt was used, phosphate adsorption was slightly higher for B880 than for B440. This may be due to B880's greater ability to retain cations, particularly Al and Fe, which was already evident in the metal uptake data. However, electrostatic attraction is likely not the only mechanism at play. Other processes, such as ligand exchange or the formation of inner-sphere complexes, especially in the presence of trivalent cations like Al^{3+} and Fe^{3+}, could also contribute to phosphate binding.

3.6. Phosphate Adsorption Isotherms and Comparison with Theoretical Models

The adsorption behaviour of phosphate onto $FeCl_3$-activated biochars (B440 and B880) was analyzed by fitting the experimental equilibrium data to three theoretical models: Freundlich, Langmuir, and Langmuir–Sips (Figure 5). The non-linear fitting of batch adsorption data (10–1000 mg P L^{-1}) provided quantitative insights into the interaction between phosphate ions and the surface of the modified biochars and enabled comparison between adsorption mechanisms.

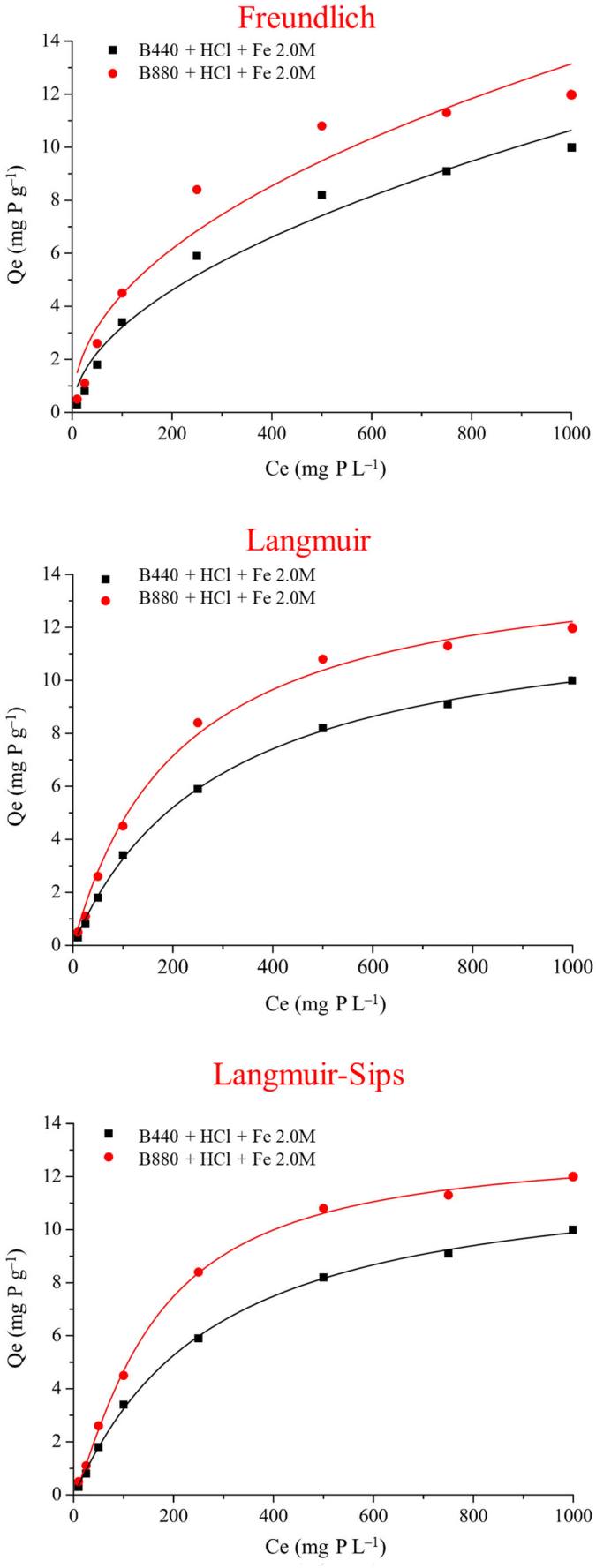

Figure 5. Adsorption isotherms for P removal by $FeCl_3$-activated biochars produced at 440 °C (B440) and 880 °C (B880), fitted using three isotherm models: Langmuir, Freundlich, and Langmuir–Sips.

The Freundlich model, which assumes heterogeneous surface adsorption with energy-distributed sites, yielded lower R^2 values (0.968 for B440 and 0.939 for B880), indicating a less precise fit (Table 4). However, the Freundlich constants confirmed a favorable adsorption process ($n > 1$) in both cases, particularly for B880 ($n = 2.1$), reflecting enhanced interaction with the more porous and metal-enriched surface. Despite its limitations, the Freundlich model provides complementary evidence of multilayer adsorption processes, especially relevant at higher phosphate concentrations.

The Langmuir model, which assumes monolayer adsorption on a homogeneous surface with finite, identical sites, produced excellent fits ($R^2 = 0.999$ for B440 and 0.994 for B880). Maximum adsorption capacities (q_{max}) were 12.9 mg P g^{-1} for B440 and 14.9 mg P g^{-1} for B880, with slightly higher affinity constants (K_L = 0.0046 L mg^{-1}) for B880 (Table 4). These results are consistent with the higher surface area, ash content, and Fe retention capacity of B880 (Table 1), all of which promote phosphate sorption. The Langmuir model thus supports the conclusion that the adsorption process on both biochars is primarily governed by chemisorption at well-defined and saturated surface sites.

Among the three, the Langmuir–Sips model, which merges the Langmuir monolayer assumption with a Freundlich-type heterogeneity parameter (n), provided the most robust fit across the full concentration range. It returned the lowest chi-square ($\chi^2 = 0.02–0.03$), highest R^2 (both 0.999), and heterogeneity indices ($n = 1.06$ for B440, 1.26 for B880) that suggest mild surface heterogeneity. The q_{max} values (12.3 and 13.1 mg g^{-1}, respectively) obtained with this model were consistent with the experimental plateau and reinforce the reliability of the fit.

Table 4. Parameter values obtained from the application of Freundlich, Langmuir, and Langmuir-Sips isotherm models. Treatments are: B440 + HCl + Fe 2.0 M and B880 -HCl + Fe 2.0 M. Values are mean ± standard deviation of three replicates.

Freundlich					
	R^2	χ^2	K_F (mg L^{-1})	-	n
B440 + HCl + Fe 2.0 M	0.968	0.5	0.3 ± 0.1	-	1.9 ± 0.2
B880 + HCl + Fe 2.0 M	0.939	1.4	0.5 ± 0.2	-	2.1 ± 0.3
Langmuir					
	R^2	χ^2	K_L (mg L^{-1})	q_{max} (mg g^{-1})	-
B440 + HCl + Fe 2.0 M	0.999	0.02	0.0034 ± 0.0002	12.9 ± 0.3	-
B880 + HCl + Fe 2.0 M	0.994	0.1	0.0046 ± 0.0005	14.9 ± 0.5	-
Langmuir Sips					
	R^2	χ^2	K_s (mg L^{-1})	q_{max} (mg g^{-1})	n
B440 + HCl + Fe 2.0 M	0.999	0.02	0.0027 ± 0.0006	12.3 ± 0.5	1.06 ± 0.05
B880 + HCl + Fe 2.0 M	0.999	0.03	0.0017 ± 0.0004	13.1 ± 0.3	1.26 ± 0.06

When compared with literature, the adsorption capacities obtained in this work fall within a moderate but consistent range. For example, Almanassra et al. [17] reviewed a broad set of studies. They concluded that Fe-enriched biochars generally achieve q_{max} values between 10 and 30 mg g^{-1}, depending on feedstock, pyrolysis conditions, and activation protocol. The consistency of our q_{max} values across both pyrolysis temperatures, together with their correlation with pH_{pzc} and surface charge modulation (Table 3), supports the mechanistic interpretation that electrostatic interactions dominate phosphate retention under acidic conditions, particularly when final pH values fall below 2 (as observed in the highest P loading). This interpretation aligns well with the results reported by Eduah et al. [27] and Yang et al. [67], who both observed maximum phosphate uptake at pH 2–3 for Fe-modified biochars.

In conclusion, while the Langmuir model provides a solid approximation of phosphate uptake by metal-activated biochars under idealized conditions, the Langmuir–Sips model emerges as the most accurate and flexible model, especially for capturing the mild heterogeneity and gradual saturation behavior observed in real systems. Its excellent fit across all concentration ranges, together with consistent mechanistic evidence (FTIR, pH_{pzc}, surface charge), confirms that $FeCl_3$ post-pyrolysis activation significantly enhances phosphate affinity, particularly for high-temperature biochars such as B880.

4. Conclusions

Activating biochar is a practical way to improve its capacity to adsorb phosphorus from aqueous solutions. The findings of this study confirm that treating biochar with chloride salts, that is, $CaCl_2$, $AlCl_3$, and $FeCl_3$, leads to effective metal uptake. As expected, higher salt concentrations resulted in greater metal absorption. Across all treatments, activated biochars outperformed the non-activated controls in terms of phosphorus adsorption, regardless of the pyrolysis temperature or the specific salt used. Among the different treatments, the highest phosphorus uptake was observed for biochar treated with 2.0 M $FeCl_3$ (10 mg P g^{-1}), followed by 2.0 M $AlCl_3$. In contrast, $CaCl_2$-treated biochars showed the lowest P adsorption performance. Overall, the amount of phosphorus retained by the activated biochars ranged from 2% to 20% of the initial P present in solution. Importantly, phosphate adsorption was strongly affected by the pH of the solution in contact with the biochar: the lower the pH, the higher the P uptake. This behavior was clearly linked to the pH_{pzc} of the biochars, which played a central role in determining whether electrostatic attraction could occur. The adsorption mechanism was found to be dominated by electrostatic interactions between anionic phosphate species and the positively charged, metal-rich biochar surfaces. This conclusion is supported by FTIR evidence, such as the disappearance of protonated O–H groups and the appearance of phosphate-related bands after adsorption, indicating phosphate binding at those activated sites. While electrostatic attraction prevailed, we do not exclude that ligand exchange or inner-sphere complexation (especially in the presence of Al^{3+} and Fe^{3+}) may also contribute to phosphate retention. These mechanistic insights, often overlooked in similar studies, underline the importance of surface charge modulation for phosphate removal.

Author Contributions: Conceptualization, V.A.L., L.B. and P.C.; methodology, V.A.L., P.C. and S.M.M.; formal analysis, S.M.M.; investigation, V.A.L. and S.M.M.; data curation, V.A.L., P.C. and S.M.M.; writing—original draft preparation, V.A.L., P.C. and S.M.M.; writing—review and editing, V.A.L., L.B. and P.C.; supervision, V.A.L. and P.C. All authors have read and agreed to the published version of the manuscript.

Funding: This research received no external funding.

Institutional Review Board Statement: Not applicable.

Informed Consent Statement: Not applicable.

Data Availability Statement: The data presented in this study are available upon request from the corresponding author.

Acknowledgments: S.M. Muscarella gratefully acknowledges the project "Achieving Wider Uptake of Water-Smart Solutions—WIDER UPTAKE" (Grant Agreement No. 869283), funded by the European Union's Horizon 2020 Research and Innovation Programme, for partially supporting her PhD studies. The UNIPA project website is available at: https://wideruptake.unipa.it.

Conflicts of Interest: The authors declare no conflicts of interest.

References

1. Tian, J.; Ge, F.; Zhang, D.; Deng, S.; Liu, X. Roles of phosphate solubilizing microorganisms from managing soil phosphorus deficiency to mediating biogeochemical P cycle. *Biology* **2021**, *10*, 156.
2. FAO. *World Fertilizer Trends and Outlook to 2022, Summary Report*; Food and Agriculture Organization: Rome, Italy, 2020.
3. van Dijk, K.C.; Lesschen, J.P.; Oenema, O. Phosphorus flows and balances of the European Union Member States. *Sci. Total Environ.* **2016**, *542 Pt B*, 1078–1093.
4. Cordell, D.; White, S. Tracking phosphorus security: Indicators of phosphorus vulnerability in the global food system. *Food Secur.* **2015**, *7*, 337–350.
5. Saliu, T.D.; Oladoja, N.A. Nutrient recovery from wastewater and reuse in agriculture: A review. *Environ. Chem. Lett.* **2021**, *19*, 2299–2316.
6. Hashem, M.S.; Qi, X. Treated wastewater irrigation—A review. *Water* **2021**, *13*, 1527.
7. Janu, R.; Mrlik, V.; Ribitsch, D.; Hofman, J.; Sedláček, P.; Bielská, L.; Soja, G. Biochar surface functional groups as affected by biomass feedstock, biochar composition and pyrolysis temperature. *Carbon Resour. Convers.* **2021**, *4*, 36–46.
8. Mannina, G.; Alduina, R.; Badalucco, L.; Barbara, L.; Capri, F.C.; Cosenza, A.; Di Trapani, D.; Gallo, G.; Laudicina, V.A.; Muscarella, S.M.; et al. Water resource recovery facilities (WRRFs): The case study of Palermo University (Italy). *Water* **2021**, *13*, 3413.
9. Fang, C.; Zhang, T.; Ping, L.; Jiang, R.; Wang, Y. Application of magnesium modified corn biochar for phosphorus removal and recovery from swine wastewater. *Int. J. Environ. Res. Public Health* **2014**, *11*, 9217–9237.
10. Wang, Y.; Munir, T.; Wu, X.; Huang, Y.; Li, B. Phosphorus recovery and reuse: Innovating with biochar in the circular economy. *Sci. Total Environ*. **2025**, *973*, 179143.
11. Nobaharan, K.; Bagheri Novair, S.; Asgari Lajayer, B.; van Hullebusch, E. Phosphorus removal from wastewater: The potential use of biochar and the key controlling factors. *Water* **2021**, *13*, 517.
12. Muscarella, S.M.; Di Trapani, D.; Laudicina, V.A.; Mannina, G. Phosphorus recovery from ultrafiltered membrane wastewater by biochar adsorption columns: The effect of loading rates. *Heliyon* **2024**, *10*, e34659.
13. Bulacio Fischer, P.T.; Di Trapani, D.; Laudicina, V.A.; Muscarella, S.M.; Mannina, G. Nutrient Recovery from Zeolite and Biochar Columns: The Case Study of Marineo (Italy) Wastewater Treatment Plant. *Water* **2025**, *17*, 848.
14. Mannina, G.; Badalucco, L.; Barbara, L.; Cosenza, A.; Di Trapani, D.; Laudicina, V.A.; Muscarella, S.M.; Presti, D. Roadmapping the transition to water resource recovery facilities: The two demonstration case studies of Corleone and Marineo (Italy). *Water* **2022**, *14*, 156.
15. Paliaga, S.; Muscarella, S.M.; Alduina, R.; Badalucco, L.; Bulacio Fischer, P.T.; Di Leto, Y.; Gallo, G.; Gaglio, R.; Mineo, A.; Laudicina, V.A.; et al. Resource recovery from wastewater treatment: Effects of water reuse and slow-release fertilizers on faba bean within Palermo University (Italy) case study. *J. Environ. Manag*. **2025**, *373*, 123839.
16. Gong, W.; Tao, C.; Tian, Z.; Huang, Z.; Lin, H.; Qi, C.; Yu, Z.; Guo, L. Characterization and mechanism of phosphorus adsorption from wastewater by lanthanum calcium doped sludge/wheat straw biochar. *Front. Environ. Sci.* **2025**, *13*, 1604542.
17. Almanassra, I.W.; McKay, G.; Kochkodan, V.; Atieh, M.A.; Al-Ansari, T. A state of the art review on phosphate removal from water by biochars. *Chem. Eng. J.* **2021**, *409*, 128211.
18. Conte, P.; Bertani, R.; Sgarbossa, P.; Bambina, P.; Schmidt, H.P.; Raga, R.; Lo Papa, G.; Chillura Martino, D.F.; Lo Meo, P. Recent developments in understanding biochar's physical–chemistry. *Agronomy* **2021**, *11*, 615.
19. Wang, Y.; Qiu, L.P.; Hu, M.F. Magnesium ammonium phosphate crystallization: A possible way for recovery of phosphorus from wastewater. *IOP Conf. Ser. Mater. Sci. Eng*. **2018**, *392*, 032032.
20. Singh, A.; Singh, A.P.; Purakayastha, T.J. Characterization of biochar and their influence on microbial activities and potassium availability in an acid soil. *Arch. Agron. Soil Sci.* **2019**, *65*, 1302–1315.
21. Pan, F.; Wei, H.; Huang, Y.; Guo, W.; Song, J.; Zhang, Z.; Teng, R.; Gao, M.; Jing, S.; Shi, B. Biochar-Enabled Phosphorus Recovery from Aqueous: Advances, Applications and Challenges. *Environ. Res*. **2025**, *285*, 122329.
22. Wu, X.; Quan, W.; Chen, Q.; Gong, W.; Wang, A. Efficient Adsorption of Nitrogen and Phosphorus in Wastewater by Biochar. *Molecules* **2024**, *29*, 1005.
23. Chen, Y.; Yang, H.; Wang, X.; Zhang, S.; Chen, H. Biomass-based pyrolytic polygeneration system on cotton stalk pyrolysis: Influence of temperature. *Bioresour. Technol.* **2012**, *107*, 411–418.
24. Luo, D.; Wang, L.; Nan, H.; Cao, Y.; Wang, H.; Kumar, T.V.; Wang, C. Phosphorus absorption by functionalized biochar: A review. *Environ. Chem. Lett*. **2022**, *21*, 497–524.
25. Ahmed, M.B.; Zhou, J.L.; Ngo, H.H.; Guo, W.; Chen, M. Progress in the preparation and application of modified biochar for improved contaminant removal from water and wastewater. *Bioresour. Technol.* **2016**, *214*, 836–851.

26. Ding, Z.; Hu, X.; Wan, Y.; Wang, S.; Gao, B. Removal of lead, copper, cadmium, zinc, and nickel from aqueous solutions by alkali-modified biochar: Batch and column tests. *J. Ind. Eng. Chem.* **2016**, *33*, 239–245.
27. Chen, M.; Liu, Y.; Pan, J.; Jiang, Y.; Zou, X.; Wang, Y. Low-cost Ca/Mg co-modified biochar for effective phosphorus recovery: Adsorption mechanisms, resourceful utilization, and life cycle assessment. *Chem. Eng. J.* **2024**, *502*, 157993.
28. Zhao, Q.G.; Li, B.; Zhou, X. Enhanced phosphate removal in water by magnesium-modified biochar/yttrium alginate hybrid biogel polymer. *J. Rare Earths* 2025, *in press*. https://doi.org/10.1016/j.jre.2025.04.018.
29. Eduah, J.O.; Nartey, E.K.; Abekoe, M.K.; Henriksen, S.W.; Andersen, M.N. Mechanism of orthophosphate (PO_4–P) absorption onto different biochars. *Environ. Technol. Innov.* **2020**, *17*, 100572.
30. Chemerys, V.; Baltrėnaitė, E. Modified Biochar: A review on modifications of biochar towards its enhanced absorptive properties. *Ann. Agric. Environ. Sci.* **2016**. Available online: https://etalpykla.vilniustech.lt/handle/123456789/117258 (accessed on 8 August 2025).
31. Choi, Y.; Jang, H.M.; Kan, E.; Wallace, A.R.; Sun, W. Absorption of phosphate in water on a novel calcium hydroxide-coated dairy manure-derived biochar. *J. Environ. Eng.* **2019**, *24*, 434–442.
32. Yang, H.; Ye, S.; Zeng, Z.; Zeng, G.; Tan, X.; Xiao, R.; Wang, J.; Song, B.; Du, L.; Qin, M.; et al. Utilization of biochar for resource recovery from water: A review. *Chem. Eng. J.* **2020**, *397*, 125502.
33. Fu, W.; Li, M.; Chen, H.; Qu, J.; Zhang, L.; Qiu, S.; Feng, M.; Yuan, M.; Guo, C.; Zhou, J.; et al. Novel utilization exploration for the dephosphorization waste of Ca–modified biochar: Enhanced removal of heavy metal ions from water. *Biochar* **2024**, *6*, 77.
34. Liu, L.; He, N.; Borham, A.; Zhang, S.; Xie, R.; Zhao, C.; Hu, J.; Wang, J. The Effect of Iron-Modified Biochar on Phosphorus Adsorption and the Prospect of Synergistic Adsorption between Biochar and Iron-Oxidizing Bacteria: A Review. *Water* **2023**, *15*, 3315.
35. Zheng, Y.; Wang, B.; Wester, A.E.; Chen, J.; He, F.; Chen, H.; Gao, B. Reclaiming phosphorus from secondary treated municipal wastewater with engineered biochar. *Chem. Eng. J.* **2019**, *362*, 460–468.
36. Zhong, Z.; Yu, G.; Mo, W.; Zhang, C.; Huang, H.; Li, S.; Gao, M.; Lu, X.; Zhang, B.; Zhu, H. Enhanced phosphate sequestration by Fe(III) modified biochar derived from coconut shell. *RSC Adv.* **2019**, *9*, 10425–10436.
37. Yin, Q.; Ren, H.; Wang, R.; Zhao, Z. Evaluation of nitrate and phosphate absorption on Al-modified biochar: Influence of Al content. *Sci. Total Environ.* **2018**, *631–632*, 895–903.
38. Sizmur, T.; Fresno, T.; Akgül, G.; Frost, H.; Moreno-Jiménez, E. Biochar modification for the removal of inorganics from water. *Bioresour. Technol.* **2017**, *246*, 33–47.
39. Sharma, R.K.; Wooten, J.B.; Baliga, V.L.; Lin, X.; Chan, W.G.; Hajaligol, M.R. Characterization of chars from pyrolysis of lignin. *Fuel* **2004**, *83*, 1469–1482.
40. Zhou, Y.; Selvam, A.; Wong, J.W.C. Chinese medicinal herbal residues as a bulking agent for food waste composting. *Bioresour. Technol.* **2018**, *249*, 182–188.
41. Munera-Echeverri, J.L.; Martinsen, V.; Strand, L.T.; Zivanovic, V.; Cornelissen, G.; Mulder, J. Cation exchange capacity of biochar: An urgent method modification. *Sci. Total Environ.* **2018**, *642*, 190–197.
42. Jones Jr, J.B.; Case, V.W. Sampling, handling, and analyzing plant tissue samples. *Soil Test. Plant Anal.* **1990**, *3*, 389–427.
43. Nasiruddin Khan, M.; Sarwar, A. Determination of points of zero charge of natural and treated absorbents. *Surf. Rev. Lett.* **2007**, *14*, 461–469.
44. Vaičiukyniene, D.; Vaitkevičius, V.; Kantautas, A.; Sasnauskas, V. Utilization of by-product waste silica in concrete-based materials. *Mater. Res.* **2012**, *15*, 561–567.
45. Murphy, J.; Riley, J.P. A modified single solution method for the determination of phosphate in natural waters. *Anal. Chim. Acta* **1962**, *27*, 31–36.
46. Canellas, J.; Soares, A.; Jefferson, B. Removing Ammonia From Wastewater Using Natural and Synthetic Zeolites: A Batch Experiment. *ChemRxiv* **2019**. https://doi.org/10.26434/chemrxiv.9831542.v1.
47. Sarioglu, M. Removal of ammonium from municipal wastewater using natural Turkish (Dogantepe) zeolite. *Sep. Purif. Technol.* **2005**, *41*, 1–11.
48. Moshoeshoe, M.; Silas Nadiye-Tabbiruka, M.; Obuseng, V. A review of the chemistry, structure, properties and applications of zeolites. *Am. J. Mater. Sci.* **2017**, *7*, 196–221.
49. Muscarella, S.M.; Laudicina, V.A.; Cano, B.; Badalucco, L.; Conte, P.; Mannina, G. Recovering ammonium by treated and untreated zeolitic mixtures: A comprehensive experimental and modelling study. *Microporous Mesoporous Mater.* **2023**, *349*, 112434.
50. Sparks, D. *Environmental Soil Chemistry*, 2nd ed.; Academic Press: Oxford, UK, 2003.
51. Liu, Y.; He, Z.; Uchimiya, M. Comparison of biochar formation from various agricultural by-products using FTIR spectroscopy. *Mod. Appl. Sci.* **2015**, *9*, 246–253.

52. Keiluweit, M.; Nico, P.S.; Johnson, M.G.; Kleber, M. Dynamic molecular structure of plant biomass-derived black carbon (biochar). *Environ. Sci. Technol.* **2010**, *44*, 1247–1253.
53. Bagreev, A.; Bandosz, T.J.; Locke, D.C. Pore structure and surface chemistry of adsorbents obtained by pyrolysis of sewage sludge-derived fertilizer. *Carbon* **2001**, *39*, 1971–1979.
54. Guo, J.; Jiang, S.; Pang, Y. Rice straw biochar modified by aluminum chloride enhances the dewatering of the sludge from municipal sewage treatment plant. *Sci. Total Environ.* **2019**, *654*, 338–344.
55. Li, X.; Qin, Y.; Jia, Y.; Li, Y.; Zhao, Y.; Pan, Y.; Sun, J. Preparation and application of Fe/biochar (Fe-BC) catalysts in wastewater treatment: A review. *Chemosphere* **2021**, *274*, 129766.
56. Panwar, N.L.; Pawar, A.; Salvi, B.L. Comprehensive review on production and utilization of biochar. *SN Appl. Sci.* **2019**, *1*, 168.
57. Zeng, S.; Kan, E. Sustainable use of $Ca(OH)_2$ modified biochar for phosphorus recovery and tetracycline removal from water. *Sci. Total Environ.* **2022**, *839*, 156159.
58. Myglovets, M.; Poddubnaya, O.I.; Sevastyanova, O.; Lindström, M.E.; Gawdzik, B.; Sobiesiak, M.; Tsyba, M.M.; Sapsay, V.I.; Klymchuk, D.O.; Puziy, A.M. Preparation of carbon absorbents from lignosulfonate by phosphoric acid activation for the absorption of metal ions. *Carbon* **2014**, *80*, 771–783.
59. Li, J.H.; Lv, G.H.; Bai, W.B.; Liu, Q.; Zhang, Y.C.; Song, J.Q. Modification and use of biochar from wheat straw (Triticum aestivum L.) for nitrate and phosphate removal from water. *Desalin. Water Treat.* **2016**, *57*, 4681–4693.
60. Yuan, J.; Wen, Y.; Ruiz, G.; Sun, W.; Ma, X. Enhanced phosphorus removal and recovery by metallic nanoparticles-modified biochar. *Nanotechnol. Environ. Eng.* **2020**, *5*, 26.
61. Antunes, E.; Jacob, M.V.; Brodie, G.; Schneider, P.A. Isotherms, kinetics and mechanism analysis of phosphorus recovery from aqueous solution by calcium-rich biochar produced from biosolids via microwave pyrolysis. *J. Environ. Chem. Eng.* **2018**, *6*, 395–403.
62. Deng, W.; Zhang, D.-Q.; Zheng, X.; Ye, X.; Niu, X.; Lin, Z.; Fu, M.; Zhou, S. Absorption recovery of phosphate from waste streams by Ca/Mg-biochar synthesis from marble waste, calcium-rich sepiolite and bagasse. *J. Clean. Prod.* **2020**, *288*, 125638.
63. Feng, Y.; Luo, Y.; He, Q.; Zhao, D.; Zhang, K.; Shen, S.; Wang, F. Performance and mechanism of a biochar-based Ca–La composite for the absorption of phosphate from water. *J. Environ. Chem. Eng.* **2021**, *9*, 105267.
64. Yao, Y.; Gao, B.; Chen, J.; Yang, L. Engineered biochar reclaiming phosphate from aqueous solutions: Mechanisms and potential application as a slow-release fertilizer. *Environ. Sci. Technol.* **2013**, *47*, 8700–8708.
65. Giménez, J.; Martínez, M.; de Pablo, J.; Rovira, M.; Duro, L. Arsenic sorption onto natural hematite, magnetite, and goethite. *J. Hazard. Mater.* **2007**, *141*, 575–580.
66. Ren, J.; Li, N.; Li, L.; An, J.K.; Zhao, L.; Ren, N.Q. Granulation and ferric oxides loading enable biochar derived from cotton stalk to remove phosphate from water. *Bioresour. Technol.* **2015**, *178*, 119–125.
67. Yang, Q.; Wang, X.; Luo, W.; Sun, J.; Xu, Q.; Chen, F.; Zhao, J.; Wang, S.; Yao, F.; Wang, D.; et al. Effectiveness and mechanisms of phosphate absorption on iron-modified biochars derived from waste activated sludge. *Bioresour. Technol.* **2018**, *247*, 537–544.

Disclaimer/Publisher's Note: The statements, opinions and data contained in all publications are solely those of the individual author(s) and contributor(s) and not of MDPI and/or the editor(s). MDPI and/or the editor(s) disclaim responsibility for any injury to people or property resulting from any ideas, methods, instructions or products referred to in the content.